Accepted Manuscript

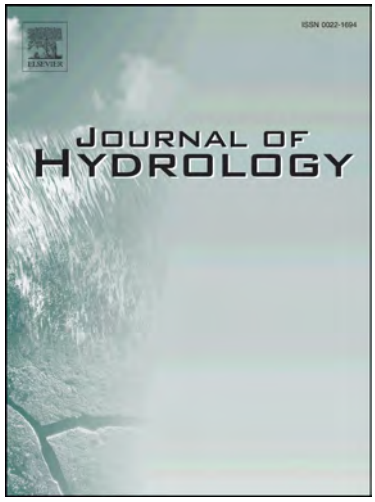

Research papers

Geochemical evolution of thermal waters in carbonate – evaporitic systems: the triggering effect of halite dissolution in the dedolomitisation and albitisation processes

M. Blasco, L.F. Auqué, M.J. Gimeno

PII: S0022-1694(19)30056-3
DOI: https://doi.org/10.1016/j.jhydrol.2019.01.013
Reference: HYDROL 23408

To appear in: *Journal of Hydrology*

Received Date: 30 August 2018
Revised Date: 4 January 2019
Accepted Date: 12 January 2019

Please cite this article as: Blasco, M., Auqué, L.F., Gimeno, M.J., Geochemical evolution of thermal waters in carbonate – evaporitic systems: the triggering effect of halite dissolution in the dedolomitisation and albitisation processes, *Journal of Hydrology* (2019), doi: https://doi.org/10.1016/j.jhydrol.2019.01.013

Geochemical evolution of thermal waters in carbonate – evaporitic systems: the triggering effect of halite dissolution in the dedolomitisation and albitisation processes

M. Blasco[a,*], L.F. Auqué[a], M.J. Gimeno[a]

[a] Geochemical Modelling Group. Petrology and Geochemistry Area, Earth Sciences Department, University of Zaragoza, Spain C/ Pedro Cerbuna 12, 50009 Zaragoza, Spain.

[*] Corresponding author: Geochemical Modelling Group. Petrology and Geochemistry Area, Earth Sciences Department, University of Zaragoza, Spain. e-mail: monicabc@unizar.es; Tel.: +34 976761071; Fax: +34 976761106.

Abstract

The Fitero and Arnedillo geothermal systems are located in the NW part of the Iberian Range (Northern Spain). The geothermal reservoir is hosted in the Lower Jurassic carbonates, in contact with the evaporitic Keuper Facies. Thermal waters are of chloride-sodium type, with discharge temperature of about 45 ºC and near neutral pH . The Arnedillo waters are more saline, with higher Na, Cl and sulphate contents, but lower Ca and Mg than the Fitero waters. All waters have attained mineral equilibrium at

depth with calcite, dolomite, anhydrite, quartz, albite, K-feldspar and other aluminosilicates, except for the Fitero waters, which have not reached the equilibrium with the aluminosilicates. The calculated reservoir temperature is 81 ± 11 ºC in Fitero and 87 ± 13 ºC in Arnedillo. In order to identify the reasons for the differences found between the two systems some inverse and forward geochemical calculations were performed and the main water-rock interaction processes responsible for the chemical evolution of these waters have been evaluated.

Halite dissolution has been found to be the triggering factor for the two most important geochemical processes in the system: a) albitisation process, due to the common ion effect (Na); and b) dedolomitisation process, associated with the salinity increase, which enhance the dissolution of anhydrite, and, in turn, produces the precipitation of calcite (common ion effect, Ca) and the concomitant dissolution of dolomite.

Halite dissolution may be an important driving force in the geochemical evolution of groundwater systems in contact with carbonates and evaporites, where equilibrium with K-feldspar, albite and anhydrite has already been attained. The evolution of the processes at pH, temperature and salinity ranges wider than those in the Fitero-Arnedillo system has been theoretically examined with additional reaction-path simulations, in order to generalise the geochemical behaviour of these processes in other environments.

Keywords: geothermal system, geothermometry, geochemical modelling, dedolomitisation, albitisation, halite dissolution triggering effects.

1. Introduction

Fitero and Arnedillo are two small villages in Navarra and La Rioja regions (Spain) respectively, which have well known spas functioning for a long time (e.g. Gutiérrez, 1801; Mezquíriz, 2004) for its medicinal and therapeutic benefits. Arnedillo is about 35 Km NW of Fitero, and the waters that emerge in both villages belong to the same carbonate-evaporitic reservoir. The discharge temperature of the thermal waters at both sites is similar, but their chemistry is different.

The hydrogeochemical characterisation of these thermal waters started with the study of the Arnedillo system (Blasco et al., 2018) and it is completed in this paper with the characterisation of the Fitero thermal waters. Moreover, following the same methodology as for the Arnedillo waters, the temperature in the reservoir of the Fitero system has been determined by using the chemical and isotopic geothermometers and the geothermometrical modelling. The use of classical chemical geothermometers (cationic geothermometers and silica geothermometers) in low-temperature and carbonate-evaporitic systems is rather controversial, since they were developed to be used in waters of higher temperature and with a different mineral assemblage in contact to the waters in the reservoir. However, although not completely free of uncertainties or limitations, there are some chemical geothermometers specifically calibrated for this type of systems (Ca-Mg and SO_4-F; Chiodini et al., 1995). These issues were thoroughly treated in the previous study on the Arnedillo waters (Blasco et al., 2018) and, therefore, only some observations are included here. In any case, as both systems belong to the same reservoir, the study of the Fitero thermal waters will improve the general understanding in the particularities of the use of these geothermometers (as explained in Blasco et al., 2017).

Finally, the geochemical characterisation of the whole system allows assessing, by mass balance and reaction paths calculations, the main reactions (and their extent) that condition the evolution of these thermal waters. This evaluation has evidenced the important role played by halite dissolution in the geochemical evolution of this type of systems through its effects on several water-mineral equilibria.

2. Geology and hydrogeology

The Fitero and Arnedillo thermal springs are located in the NW of the Iberian Chain, in the contact between the eastern Cameros Range and the tertiary Ebro Basin (Figure 1; Coloma et al., 1997; Sánchez and Coloma, 1998). These springs are aligned in a NW-SE thrust that separates the aforementioned two units (Albert, 1979; Auqué et al., 1988). They are located in the Fitero (Navarra, Spain) and Arnedillo (La Rioja, Spain) villages, respectively, which are separated by about 35 km.

The Cameros Range, constituted mainly by Mesozoic rocks, is limited by two continental basins and two Palaeozoic reliefs (Figure 1): the Ebro and Duero basins in the north and the south, respectively; and the Demanda and Moncayo Ranges at the east and west (Gil et al., 2002). The formations of this area range from the Paleozoic up to the Quaternary. The Triassic and the marine Jurassic carbonate rocks (up to Kimmeridgian) constitute the pre-rift sequence, and they are represented by the formations normally found in the Iberian Chain (Coloma, 1998; Gil et al., 2002; Goy et al., 1976). At the end of the Jurassic and during the Cretaceous time a rifting process resulted in the creation of the Cameros Basin and the sedimentation of this period constitute the syn-rift sequence. These are continental sediments from Upper Jurassic to Upper Cretaceous (Tithonian to Lower Albian; Coloma, 1998; Gil et al., 2002; Mas et al., 1993) and they are constituted by an intercalation of fluvial and lacustrine sediments. Finally, the post-rift sequence is constituted by the Upper Cretaceous

carbonates (Urgon Facies) and sandstones (Utrillas Formation) and the carbonates of the Later Cretaceous (Santa María de la Hoyas, Picofrentes, Muñecas, Hortezuelos, Hontoria Pinar, Burgo de Osma, Santo Domingo de Silos, Santibañez del Val Formations; Gil et al., 2002, 2004). The Cameros Range relief and the tertiary basin were created during the tertiary tectonic inversion when E-W and NW-SE compressive structures, such as the Cameros thrust, were generated (Coloma, 1998; Gil et al., 2002).

The geothermal reservoir associated with these thermal waters is located in the Jurassic carbonates of the pre-rift sequence. Based on their permeability, these materials have been divided in three groups, two permeable ones separated by other less permeable (Coloma et al., 1995; Sánchez and Coloma, 1998; Sánchez et al., 1999), although they are interconnected due to the intense fracturation:

1) Group 1 (the first permeable group): Imón (dolostones), Cortes de Tajuña (dolomitic carnioles) and Cuevas Labradas (limestones and dolostones) Formations.

2) Group 2 (the intermediate less permeable group): Cerro del Pez (marls), Barahona (bioclastics limestones) and Turmiel (marls and limestones) Formations.

3) Group 3 (the second permeable group): Chelva (limestones), Aldealpozo (black limestones) and Torrecilla (limestones with corals) Formations.

All these formations constitute the regional drainage level of the Iberian Chain, although the main flow occurs through the materials of the first permeable group (Coloma et al., 1995; Sánchez and Coloma, 1998; Sánchez et al., 1999).

The recharge occurs through the outcrops of Jurassic rocks and the syn-rift sequence and from the infiltration from rivers (Coloma et al., 1995; Sánchez et al., 1999). Then, the ascent of the thermal waters to the surface takes place through the Cameros thrust (Coloma, 1998; Coloma et al., 1996; Figure 1). The discharges are associated with the Keuper facies by Lower Jurassic formations (Auqué et al., 1988; Coloma, 1998;

Coloma et al., 1996). The thermal waters are of chloride-sodium type and the discharge temperature is close to 50 ºC in both cases, however, the flow rate is higher in Fitero (about 50 L/s) than in Arnedillo (up to 20 L/s; Coloma et al., 1998, 1997b, 1995; Sánchez and Coloma, 1998).

3. Methodology

3.1. Field sampling and analyses

A sampling campaign was conducted in October 2015 and four water samples were taken and analysed. Two of them were collected in Arnedillo, one inside the Arnedillo spa (AR1) and the other in a spring in a pool built in the Cidacos River (AR2). The other two samples were taken in Fitero in two different spas, one in the Bequer spa (F1) and the other in the Palafox spa (F2).

The field sampling procedures and analytical methodology were described in detail in Blasco et al. (2018). Briefly, temperature, pH and electrical conductivity were determined in situ in all these samples; alkalinity was determined by titration with H_2SO_4 0.02N and endpoint monitoring by pH-meter, chloride and fluoride by selective electrodes and sulphates by colorimetry. The major cations (Ca, Na, K, Mg, Sr and Si) were analysed by ICP-OES, the minor cations by ICP-MS and the isotopes ($\delta^{18}O$, $\delta^{2}D$, $\delta^{13}C$, and $\delta^{34}S$ and ^{18}O in dissolved sulphates) by CF-IRMS.

3.2. Geothermometers

The use of chemical and isotopic geothermometers for determining the reservoir temperature of a thermal system can be considered complementary to the geothermometrical modelling and through the combination of the three techniques the temperature is more precisely established. The characteristics of the chemical and isotopic geothermometers used here and their application to these thermal waters were

detailed in Blasco et al. (2018), so here only the most relevant information is highlighted.

3.2.1. Chemical geothermometers

Chemical geothermometers are the classical technique used for determining the reservoir temperature of thermal waters. They consist of empiric or experimental calibrations based on chemical heterogeneous reactions which depend on temperature and control the elemental contents dissolved in waters (e.g. Marini, 2004; Truesdell, 1976). There are some geothermometers that have specifically been calibrated for carbonate-evaporitic and low temperature thermal systems and they have been used in this study: the Ca-Mg and the SO_4-F geothermometers (Chiodini et al. 1995).

However, most of the existing geothermometers (cationic and silica geothermometers) have been calibrated for waters of high temperature (>180 ºC) and hosted in different rocks than the ones present in the studied area (e.g. Arnòrsson et al., 1983; Asta et al., 2010; Auqué et al., 1997; Buil et al., 2006; Choi et al., 2005; D´Amore et al., 1987; Fouillac and Michard, 1981; Fournier, 1981, 1977; Giggenbach et al., 1983; Giggenbach, 1988; Kharaka and Mariner, 1989; Mariner et al., 2006; Mutlu and Güleç, 1998; Stefánsson and Arnórsson, 2000). These geothermometers have provided coherent results in some systems similar to the ones studied here (e.g. Apollaro et al., 2012; Blasco et al., 2018, 2017; Fernández et al., 1988; Gökgöz and Tarkan, 2006; Michard and Bastide, 1988; Mohammadi et al., 2010; Pastorelli et al., 1999; Wang et al., 2015) and, therefore, their applicability in the Fitero – Arnedillo geothermal system is tested. Classical chemical geothermometers and calibrations used in this study are: SiO_2-quartz (calibrations: Fournier, 1977; Michard, 1979; Truesdell, 1976), SiO_2-chalcedony (calibrations: Arnòrsson et al., 1983; Fournier, 1977) Na-K (calibrations:

Fournier, 1977; Giggenbach, 1988; Verma and Santoyo, 1997), K-Mg (Giggenbach et al., 1983 calibration) and Na-K-Ca (Fournier and Truesdell, 1973 calibration).

3.2.2. Isotopic geothermometers

Isotopic geothermometers are similar to chemical geothermometers as they consist of reactions dependent on temperature, however they are based on the isotopic equilibrium between two species. The isotopic geothermometers used in this study are the ones based on the $\delta\ ^{18}O$ exchange between waters and sulphate. The traditional calibrations for this geothermometer are based on the $\delta^{18}O$ HSO_4-H_2O exchange and the calibrations used here are those from Friedman and O'Neil (1977) and Seal et al. (2000). However as isotopic equilibrium in waters of neutral pH is supposed to be controlled by the $\delta^{18}O$ SO_4^{2-}-H_2O exchange (Boschetti, 2013), additional calibrations based on this assumption have also been used (Halas and Pluta, 2000; Zeebe, 2010). Finally, the calibration based on $\delta\ ^{18}O$ $CaSO_4$-H_2O exchange (Boschetti et al., 2011) provides good results in systems oversaturated or in equilibrium with anhydrite (e.g. Awaleh et al., 2015; Boschetti, 2013; Boschetti et al., 2011) and it has also been used here.

3.3. Geochemical modelling

The geochemical calculations have been performed by using the PHREEQC geochemical code (Parkhurst and Appelo, 2013) and the WATEQ4F thermodynamic database (Ball and Nordstrom, 2001) with some additional thermodynamic data which are detailed below:

- pyrophyllite, laumontite, albite, K-feldspar and chalcedony data from Michard (1983). These data have been selected because they have provided good results in geothermal systems previously (e.g. Asta et al., 2012; Auqué et al., 1998;

Michard and Roekens, 1983; Michard et al., 1989, 1986b) and their reliability in this system was proven by Blasco et al. (2018); and

- dolomite data from Blasco et al. (2018), which was calculated from the data of the Arnedillo geothermal system. This is a partially ordered dolomite which consists of 18.4% of ordered dolomite and 81.6% of disordered dolomite.

3.3.1. Speciation-solubility calculations

These calculations provide the distribution of the different species in the water, determining their concentrations and activities. They also give the saturation states of waters with respect to the mineral phases and the partial pressure of gasses (e.g. pCO_2). The saturation state (SI) is the logarithm of the ratio between the ionic activity product (IAP) and the equilibrium constant of the mineral reaction at the indicated temperature (K(T)):

$$SI = log\left(\frac{IAP}{K(T)}\right) \quad (1)$$

When SI = 0 the solution is in equilibrium with the mineral phase, a positive value indicates oversaturation and a negative value undersaturation. These determinations will be the basic part of the geothermometrical modelling.

3.3.2. Geothermometrical modelling

As mentioned above, in order to compare the results, the geothermometrical techniques used here are the same as the ones used to estimate the reservoir temperature of the Arnedillo thermal waters (Blasco et al., 2018): chemical and isotopic geothermometers (that will be described further) and geothermometrical modelling (or multicomponent solute geothermometry; e.g. Spycher et al., 2014). With this last technique, the temperature of the reservoir is determined by simulating an increase of the temperature

of the thermal water to find the temperature range at which the saturation states of a previously selected mineral set (according to the reservoir mineralogy and assuming that they will be in equilibrium in the reservoir) reach equilibrium simultaneously. A more detailed explanation of this method and the minerals selected for the modelling can be found in Blasco et al. (2018).

3.3.3. Inverse and direct modelling

Mass-balance calculations (inverse modelling) provide the mass transfer for the selected or assumed reactions between two connected points of the system along a flow path but without taking into account the thermodynamic feasibility of those reactions (Back et al., 1983; Busby et al., 1991; Hanshaw and Back, 1985; Plummer and Back, 1980; Plummer, 1977; Plummer et al., 1990, 1983; Román-Mas and Lee, 1987; Zhu and Anderson, 2002). In this case the assumption is that Fitero and Arnedillo are geochemically related and, although they are not strictly in the same flow path, they represent two different evolution stages, that is, Fitero will be considered as the initial solution and Arnedillo the final one. The mass transfers that will be obtained with this assumption will be used in a qualitative way to assess the differences in the intensity of the reactions controlling the chemistry of the thermal waters. To solve a mass balance calculation the necessary data include: the chemical composition of the initial and the final waters and the mineral and gas phases which the waters can react with while moving from the initial to the final point. The most feasible model obtained with this calculation will be selected according to the geochemical characteristics of waters and the thermodynamic feasibility of the mass transfers obtained, which is then checked with a reaction-path simulation.

Reaction path-modelling (forward or direct modelling) checks the thermodynamic feasibility of the previous mass balance models. The initial water from the mass balance

is taken as the starting point and its evolution is simulated imposing the reactions obtained previously. The results indicate the theoretical composition of the final water together with the amount of precipitated or dissolved phases. The coherence of the inverse and direct modelling results will support the conclusion on which are the most feasible reactions taking place in the system.

4. Results and discussion

4.1. Chemical and isotopic characteristics of the waters

The four samples collected in 2015 have been considered in this study, two from Fitero and two from Arnedillo. The detailed study of the Arnedillo samples can be found in Blasco et al. (2018) and they will be discussed here in comparison with the Fitero waters.

All these thermal waters are of chloride – sodium type, with pH between 6.86 and 7.11 and spring temperature about 45 ºC (except for AR2 which is 39.5 ºC due to its location in the Cidacos river with which some mixing happens; Table 1). The most important differences between the Fitero and the Arnedillo waters are those related to their salinity and their Al contents, in general lower in Fitero:

1. The total dissolved solids (TDS) in Fitero thermal waters is about 4800 ppm while in Arnedillo is higher, about 7500 ppm.
2. Dissolved Cl and Na contents are almost half in Fitero (about 1600 and 1000 ppm, respectively; Table 1) than in Arnedillo (about 3000 and 2000 ppm, respectively; Table 1).
3. The aluminium is lower in the samples from Fitero than in the samples from Arnedillo.
4. Dissolved F, SO_4 and SiO_2 are higher in the Arnedillo samples.

5. Only dissolved Ca, Mg and K are higher in the Fitero samples.

With respect to the molar ratios, the main observations are:

1. Despite the difference in the salinity of the waters the Na/Cl molar ratio is close to 1 in all the samples (Table 1) which indicates that the Na and Cl concentrations are mainly controlled by halite dissolution, although, considering the concentration values, the amount of dissolution is higher in the Arnedillo waters.
2. The Ca/SO_4, and $Ca+Mg/HCO_3+SO_4$ ratios (the last one in eq/L) are quite similar for all samples although slightly higher in Fitero.
3. The Ca/SO_4 molar ratio is about 0.82 in Fitero and about 0.69 in Arnedillo (Table 1). Considering that anhydrite is the main control for the SO_4 contents, the value of this ratio lower than 1 means that Ca is being removed from waters by the carbonate precipitation, which (based on the value) would be higher in the case of Arnedillo.
4. The values for the $Ca+Mg/HCO_3+SO_4$ ratio (in eq/L) are 0.98 in Fitero and 0.81 in Arnedillo (Table 1). The fact that this ratio is lower than 1, mainly in the Arnedillo thermal waters, means that, apart from the role played by calcite, dolomite and anhydrite, other processes should be involved in the control of this ratio.
5. Finally, the similar values found in the two systems for the Mg/Ca molar ratios (0.28 in Fitero and 0.24 in Arnedillo) and the aMg/aCa activity ratios (0.29 in Fitero and 0.26 in Arnedillo) suggest a similar calcite – dolomite equilibrium temperature in the reservoir.

The differences found between the Fitero and the Arnedillo samples, along with their similarities, are coherent with the fact that the thermal waters from both sites belong to

the same geothermal reservoir, although with a more evolve stage of water-rock interaction in the case of Arnedillo thermal waters.

This hypothesis is also supported by some of the isotopic data of the waters. Tritium was not analysed in these samples, but Coloma et al. (1997a) reported values of 0.8 ± 2.5 TU and 7 ± 1.5 TU in the Fitero spas and 1.1 ± 2.5 TU in the Arnedillo spa. This low content of tritium suggests that the recharge of the waters was prior to 1952, when the thermonuclear testing began, and are not affected by mixing with recent waters, except for the sample from Fitero with 7 ± 1.5 TU, in which a low proportion of mixing can exist (Clark and Fritz, 1997).

The values of $\delta^{18}O$ – $\delta^{2}H$ in these samples (Table 1) indicate a meteoric origin of the waters since the $\delta^{18}O$ – $\delta^{2}H$ ratio represented in Figure 2 is close to the Global Meteoric Water Line ($\delta^{2}H = 8 \cdot \delta^{18}O + 10$; Craig, 1961) and to the Spanish Meteoric Water Line calculated from the data of the Spanish Network for the control of the isotopes in the rainfall (Díaz-Teijeiro et al. 2009; $\delta^{2}H = 8 \cdot \delta^{18}O + 9.27$). The similar $\delta^{18}O$ and $\delta^{2}H$ values for all the water samples suggest that their recharge area is the same, supporting the hypothesis of Fitero and Arnedillo waters belonging to the same geothermal reservoir.

The main sources for the $\delta^{13}C$ of the waters are: 1) the organic matter present in the soil through which the waters recharge, which has values that range from -24 to -30 ‰ for the C3 plants (the most likely ones to exists in the area, promoting a mean $\delta^{13}C$ value for the soil CO_2 of -23 ‰; Clark and Fritz, 1997) and 2) the interaction with carbonates, whose $\delta^{13}C$ is approximated to be 0 ‰ (see Blasco et al., 2018 and references therein for a more complete explanation). Therefore, the higher the $\delta^{13}C$ value, the higher the interaction with the dissolved carbonates of the waters. The $\delta\ ^{13}C$ in the dissolved inorganic carbon (DIC) in the Arnedillo waters is higher than in the Fitero ones (about -

5 ‰ and -8.4 ‰ respectively; Table 1) indicating that the thermal waters from Arnedillo have had a greater (or longer) interaction with carbonates than the thermal waters from Fitero.

Finally, the values of $\delta^{34}S$ and $\delta^{18}O$ in the dissolved sulphate are nearly the same for the Fitero and Arnedillo waters, being of about 14.8 ‰ for the $\delta^{34}S$ and 14‰ for the $\delta^{18}O$ (Table 1). As explained in Blasco et al. (2018) these values agree with those reported for the Keuper facies in the surrounding areas indicating that these thermal waters have been in contact with these rocks in the reservoir.

4.2. Saturation indices

The speciation-solubility results obtained at spring temperature for the Fitero thermal waters are very similar to the ones obtained for the Arnedillo samples discussed in Blasco et al. (2018). The main results concerning the carbonate phases, fluorite, evaporitic phases and silica and silico-aluminate phases, are described and compared next.

Thermal waters are almost in equilibrium (slightly oversaturated) with respect to calcite except for the sample F2 which is more oversaturated (Table 2). Dolomite is oversaturated in F2, less oversaturated in F1 and AR2 and slightly undersaturated in AR1. The log pCO_2 is higher than the atmospheric value in all the cases, -1.6 in F1 and AR1 and about -1.81 in F2 and AR2, which might produce CO_2 outgassing process with variable intensity and carbonate phases saturation states with variable values in the springs.

All the waters are undersaturated with respect to fluorite and to the evaporitic phases. However, fluorite is more undersaturated in Fitero while the saturation states of anhydrite and gypsum are quite similar in both systems (between -0.4 and -0.5 in the

case of anhydrite and between -0.3 and -0.37 in the case of gypsum). Finally, all the samples are highly undersaturated with respect to halite.

Quartz and chalcedony are slightly oversaturated in all thermal waters, although the Fitero samples are closer to equilibrium, especially with chalcedony (IS = 0.02 and 0.03). Finally, all the samples are oversaturated with respect to the aluminosilicate phases considered in the calculations: albite, K-feldspar, kaolinite, pyrophillite and laumontite. The only exception is the case of laumontite which is undersaturated in the Fitero samples. In all cases, the saturation states of the aluminosilicate phases are higher in the Arnedillo waters, probably associated with their higher dissolved aluminium contents (Table 1).

4.3. Geothermometry

4.3.1. Chemical geothermometers

Table 3 shows the results obtained for the samples considered in this study by using various chemical geothermometers. Compared with the Arnedillo results, the temperatures obtained with the silica geothermometers are lower in the Fitero samples. The SiO_2-quartz geothermometer provides a temperature of about 80 ºC for the Arnedillo samples and about 70 ºC for the Fitero ones. A similar situation occurs with the SiO_2-chalcedony geothermometers, giving a temperature of 50 ºC for Arnedillo and of 40 ºC for Fitero. This temperature is similar or lower than the discharge temperature and therefore, the phase most likely controlling the dissolved silica contents is quartz and not chalcedony in both systems.

Despite having provided coherent results in Arnedillo thermal waters, some of the cationic geothermometers provide too high temperatures in the case of Fitero. The calibrations considered for the Na-K geothermometer provide temperatures in the range

of 133 – 160 ºC. This geothermometer is usually considered inappropriate for low temperature carbonate evaporitic systems because waters are not expected to reach the equilibrium with the mineral phases on which they are based. This situation has been checked with the Giggenbach diagram (Figure 3), where Arnedillo thermal waters are plotted in the field of partially equilibrated waters whereas Fitero thermal waters are close to the immature waters field. This different behaviour supports again the hypothesis of different local flow paths or residence times in the geothermal reservoir.

From the cationic geothermometers only the K-Mg provides temperatures similar to those obtained with the SiO_2-quartz geothermometers, close to 70 ºC. These two geothermometers have been identified in previous studies as the most suitable for low temperature carbonate-evaporitic systems (e.g. Apollaro et al., 2012; Pastorelli et al., 1999; Wang et al., 2015).

The results obtained with the rest of the geothermometers (Na-K-Ca and Ca-Mg) indicate higher temperatures. The Na-K-Ca (with $\beta = 4/3$ as recommended by Fournier and Truesdell, 1973) provides results of 91 and 92 ºC for the Fitero waters which are higher than expected (according to the results obtained with the SiO_2-quartz geothermometers the expected results should be lower than in the Arnedillo waters); however, these results are in the accepted uncertainty range for these calculations (± 20 ºC; Fournier, 1982) and, therefore, they will be taken into account. The Ca-Mg geothermometer provides even higher temperatures (close to 110 ºC) which are not coherent with the rest of values despite the fact that in a carbonate evaporitic system the equilibrium calcite-dolomite is expected to exist. Therefore, this higher temperature is probably due to the uncertainties associated with the order degree of dolomite (Chiodini et al., 1995) or to other secondary processes affecting the dissolved Ca or Mg contents. Finally, as previously indicated in Blasco et al. (2018), the SO_4-F geothermometer

provide incoherent results (negative temperatures; Table 3) since fluorite is not likely to be in the reservoir in amounts enough to control the contents of the waters.

Considering all these results and excluding the higher and the lower results previously mentioned, the temperature obtained for the Fitero reservoir with the chemical geothermometers is of 81 ± 11 ºC, which is slightly lower than the temperature previously deduced for Arnedillo thermal waters (87 ± 13 ºC).

4.3.2. Isotopic geothermometers

The results provided by the isotopic geothermometers are very similar for Fitero and Arnedillo thermal waters (Table 3), since the isotopic values are also very similar (Table 1):

1. The temperatures obtained with the calibrations based on the equilibrium exchange between HSO_4^- and H_2O are in the range of 60 – 69 ºC for the four samples.
2. The calibrations based on the equilibrium exchange between the SO_4^{2-} and H_2O provide too low and incoherent temperatures, between 14 and 25 ºC.
3. The calibration based on the equilibrium exchange between anhydrite ($CaSO_4$) and H_2O (Boschetti, 2013), provides temperatures between 70 and 75 ºC.

The temperatures obtained with this last calibration ($CaSO_4$-H_2O exchange) are the most reasonable ones since anhydrite is in equilibrium in the system (see below) and, they are in the range previously defined with the chemical geothermometers. The bad results obtained with the calibration based on SO_4^{2-} (despite being the dominant sulphur species in this type of waters), are probably due to the lack of equilibrium between SO_4^{2-} and H_2O (Blasco et al., 2018, 2017; Boschetti et al., 2011). On the contrary, although, the HSO_4 is not the main species, the calibration based on it provides good

results because it is very similar to the $CaSO_4$-H_2O calibration in a $10^3 ln\alpha - 10^6/T^2$ plot (see Blasco et al., 2018).

4.3.3. Geothermometrical modelling

The geothemometrical modelling of the Fitero waters shows that most of the minerals reach equilibrium at the range temperature between 71 and 82 ºC, which agrees with the previous results obtained with the chemical and isotopic geothermometers. However, as already observed in the case of the Arnedillo samples (Blasco et al., 2018), calcite, dolomite and chalcedony reach equilibrium at a lower temperature: chalcedony indicates a temperature of about 50 ºC, calcite of 29 ºC for F1 and a negative temperature for F2, and dolomite of 47 ºC for F1 and 23 ºC for F2. Albite and K-feldspar also reach equilibrium at low temperature, about 50 and 60 ºC, respectively. The lower equilibrium temperature obtained for chalcedony confirms that the phase controlling the dissolved silica in these thermal waters is quartz. Considering that calcite and dolomite should be in equilibrium in this geothermal system, the lack of agreement with the rest of the mineral assemblage must be related to an outgassing process during the ascent of thermal waters to surface, as it also occurs in the Arnedillo system (the log pCO_2, is much higher than the atmospheric value, Table 2; Blasco et al., 2018). To reconstruct the conditions of thermal waters at depth an increase of the CO_2 partial pressure from 3.4 mmol/l in F1 and 3.2 mmol/L in F2 up to 4.9 mmol/L (pH = 6.3) has been simulated as it was done in Arnedillo (5 mmol/L in that case; Blasco et al., 2018) following the recommendations from Pang and Reed (1998) and Palandri and Reed (2001). The amount of CO_2 added is the necessary to adjust the calcite equilibrium temperature in the same range as the rest of the minerals (calcite is used instead of dolomite since it is less affected by thermodynamic uncertainties). Figure 4 and Table 4 show the results obtained with the geothermometrical modelling after the reconstruction

of the water conditions at depth (the Arnedillo results have also been included in the table).

The results obtained from the aluminosilicate phases for the Fitero thermal waters are almost the same for both samples and slightly lower than those obtained for Arnedillo. The phases considered in the modelling (albite, K-feldspar and pyrophillite) provide a low temperature (Figure 4 and Table 4). One possible reason for this result can be related to the very low aluminium concentration in the Fitero waters. In order to ascertain whether this lower aluminium concentration was due to an analytical error, the aluminium analyses were repeated in a different laboratory obtaining the same range of values. Additionally several theoretical simulations have been performed increasing the aluminium content of the waters (Figure S1 of the supplementary material) and the results suggest that thermal waters are in real disequilibrium with respect to the aluminosilicate phases, since the amount of aluminium necessary to make the saturation state to converge with albite and K-feldspar (providing a temperature about 100 ºC), would be 0.4 ppm (see the explanation presented in the supplementary material) which is much higher than the concentrations measured in the Arnedillo waters (0.01 to 0.06 ppm), where these phases are close to equilibrium. This is coherent with the results obtained with the chemical geothermometres, which also suggest the disequilibrium of Fitero thermal waters with respect to the aluminosilicate phases.

After this discussion the main results indicate that, without considering the aluminosilicate phases, since they do not represent an equilibrium situation, the temperature predicted for the Fitero samples is in a range between 71 and 84 ºC, that is, 78 ± 7 ºC. This result is in clear agreement with the previously obtained with the chemical and isotopic geothermometers. Combining all the results, a reliable range of temperature of 81 ± 11 ºC for the reservoir of the Fitero thermal waters can be

established. This temperature is similar, although slightly lower, than the temperature deduced for the reservoir of Arnedillo thermal waters, 87 ± 13 ºC, by Blasco et al. (2018).

4.3.4. Geochemical modelling

As mentioned above, thermal waters that emerge in the Fitero and Arnedillo springs show similar chemical and physico-chemical characteristics but also some differences suggesting that, although belonging to the same reservoir, their exact flow paths and/or their residence times differ and they undergo different intensities of water-rock interaction processes. According to the results shown in this paper, the Fitero thermal waters are less saline and more immature than thermal waters in Arnedillo. Thus, although they are not directly connected, an evolutionary geochemical path from the chemical characteristics represented by the Fitero thermal waters towards the more evolved Arnedillo thermal waters is interpreted to exist in the reservoir.

Inverse and direct modelling calculations have been performed (using one sample from each system, AR1 and F1) to assess the possible water-rock interaction processes responsible for the evolution and their intensities. The simplest calculation is the inverse modelling (mass balance) only considering the chemical characteristics of the waters (see Table 1 and compare the chemical values of the samples), which identify the most probable mass transfers in the reservoir. Then the results obtained with this calculation and their interpretation will be checked and completed with the direct modelling (reaction path). These two types of calculations have been performed considering the following assumptions:

- The mineral phases which the waters can interact with are: halite, anhydrite, calcite, dolomite, quartz, albite and K-feldspar.

- Cation exchange involving Na, Ca and Mg is also considered in the models.
- In order to reproduce the conditions at depth, the characteristics of the thermal waters have been adjusted according to the following: a) the calculations have been performed at the temperatures calculated for the reservoir; b) the amount of CO_2 (and, therefore, the pH values) has been modified to avoid the effect of the CO_2 outgassing in surface; and c) the waters have been equilibrated with the minerals found in equilibrium at the reservoir temperature (i.e. the Fitero water has been equilibrated with calcite, dolomite, anhydrite and quartz at 81 ºC, and the Arnedillo water has been equilibrated with calcite, dolomite, anhydrite, quartz, albite and K-feldspar at 87 ºC).

4.3.5. Mass-balance calculations

These calculations have been performed with the inverse modelling capacities of PHREEQC taking the Fitero waters (F1) as initial solution and the Arnedillo waters (AR1) as final solution. The uncertainty allowed in the calculations is 3% (see Parkhurst and Appelo, 2013 for more details). Sixteen models have been obtained (Table 5) indicating the following mass transfers:

1. The highest mass transfer found in the models is the dissolution of about 45 mmol/L of halite.
2. About 1.4 mmol/L of anhydrite dissolves.
3. 0.56 mmol/L of albite precipitate in all models and almost the same amount of K-feldspar dissolves indicating an albitisation process.
4. Some models do not show any mass transfer affecting quartz but in others, a small dissolution occurs (0.07 mmol/L).

5. The results for calcite and dolomite are more variable in the various models: a) no mass transfer for calcite but dolomite dissolution (lower than 0.05 mmol/L); b) no mass transfer for dolomite but calcite dissolution (always lower than 0.1 mmol/L); c) calcite dissolution (about 1.2 mmol/L) and dolomite precipitation (about 0.5 mmol/L); and d) dolomite dissolution and calcite precipitation (a dedolomitisation process), which are the cases in which the higher mass transfer takes place (about 2.5 mmol/L of dissolved dolomite and 5 mmol/L of precipitated calcite).
6. Finally, the Na exchanger (NaX) releases about 6 mmol/L and the Ca and Mg exchangers (CaX_2 and MgX_2), in some cases, remove these elements from the waters in different ways: a) CaX_2 removes about 2.4 mmol/L and MgX_2 about 0.6 mmol/L; b) CaX_2 removes about 3 mmol/L and there is no transfer affecting MgX_2; and c) MgX_2 removes about 3mmol/L and there is no transfer affecting CaX_2.

Compared with the expected mass transfers and reactions than can be deduced from the elemental differences between the initial and final solutions (Table 1), the following conclusions can be indicated:

- Chloride content in Arnedillo is 46 mmol/L higher than in Fitero and halite is assumed to be the only control of this element. The results obtained in all the models agree with this.
- Sulphate content in the Arnedillo water is about 2 mmol/L higher than in Fitero, and anhydrite seems to be the only controlling mineral for dissolved sulphate. Therefore, although the waters in both systems are in equilibrium with respect to anhydrite, this mineral seems to be dissolving due to the changes in salinity produced by halite dissolution (e.g. Li and Duan, 2011).

- Anhydrite dissolution will increase the calcium content of waters leading to the oversaturation and precipitation of calcite, which will explain the slightly lower contents of calcium in the Arnedillo waters (Table 1). Calcite precipitation causes an increase in the H^+ and the pCO_2 producing the dissolution of dolomite. This situation will explain the lower pH and higher pCO_2 (when the conditions at depth are theoretically reconstructed) in Arnedillo thermal waters. As a result, only the models that consider a dedolomitisation process seem to be plausible (Table 5).
- The dedolomitisation would also produce an increase in the dissolved magnesium in Arnedillo thermal waters which is not observed (Table 1). Therefore, an additional process should be removing the magnesium from the waters. The Mg sink that other authors have considered as the most likely in systems where dedolomitisation was also the driving process (e.g. Madison Aquifer; Busby et al., 1991; Jacobson and Wasserburg, 2005; Plummer et al., 1990) is the existence of a cationic exchange process where Na is released to the waters while Mg or Mg + Ca are uptaken. This situation also seems to be the most probable one in this system and it is coherent with some of the models obtained (those in which the dedolomitisation also takes place; Table 5).
- Finally, the increase of the Na dissolved contents as a result of halite dissolution can produce the albite precipitation which is associated with the K-feldspar dissolution (albitisation process).

In summary, the main processes responsible for the chemical evolution of these waters in the geothermal reservoir seem to be the dedolomitisation and albitisation processes and their thermodynamic feasibility will be checked with the reaction-path calculations.

4.3.6. Reaction-path calculations

These calculations will consider the dedolomitisation and albitisation processes triggered by halite and anhydrite dissolution; to make the calculations simple, the cationic exchange is not included because the information that would be necessary (amount of exchangers and their exchange capacity) is not available and its consideration is not decisive for the verification of the feasibility of the main processes.

The first reaction-path calculation consisted of forcing the Fitero waters (F1), at 81 ºC, to dissolve 46 mmol/L of halite while mineral equilibria with calcite, dolomite, quartz, anhydrite, albite and K-feldspar is maintained.

The thermodynamic results show a small precipitation of quartz (0.01 mmol/L), dissolution of anhydrite, K-feldspar and dolomite, and precipitation of albite and calcite. That is, the simulations evidence that the addition of NaCl (i.e. halite dissolution) produces albitisation and, especially, dedolomitisation, supporting the conclusions obtained previously from the mass balance calculations and excluding the rest of the obtained mass balance models. The obtained mass transfers are shown in Table 6 and Figure 5, and the changes produced in the elemental contents are shown in Figure 6. The composition of the final water obtained after the reaction path calculation (Table 6) is quite similar to the composition of the Arnedillo water at depth. Dedolomitisation processes have been identified in groundwater systems at very different depths and conditions: in shallow, low temperature and fresh water environments (e.g. Bischoff et al., 1994; Cañaveras et al., 1996; López-Chicano et al., 2001; Moral et al., 2008), in deeper aquifers and thermal waters with variable salinity (e.g. Auqué et al., 2009; Back et al., 1983; Blasco et al., 2017; Frondini, 2008; Plummer et al., 1990; Prado-Pérez and Pérez del Villar, 2011) and even in brines during burial diagenesis (e.g. Budai et al., 1984; Stoessell et al., 1987; Woo and Moore, 1996 and references therein).

Albitisation processes (like the K-feldspar albitisation deduced in this study) are usually developed in groundwater systems at temperatures higher than 60 ºC (e.g. Aagaard et al., 1990) but they have also been observed in thermal waters at similar temperatures (around 85 ºC) and salinities (TDS about 8000 ppm) to the ones studied here (Blasco et al., 2018) or, more often, in more saline formation or interstitial waters in sedimentary basins at higher temperatures (e.g. Aagaard et al., 1990; Dias Lima and De Ros, 2002; Egeberg and Aagaard, 1989; Hanor, 1996; Saigal et al., 1988 and references therein). That is, the two main processes identified in this system can take place in other situations and under different pH (pCO_2), temperature and salinity conditions.

In order to make these findings more general, some additional simulations have been performed to assess the effects of different physicochemical conditions on the main processes identified (dolomitisation and albitisation). For this, sample F1 has been considered as the initial solution and it has been forced to dissolve up to 2000 mmol/L of halite (ionic strength close to 2).Then the various conditions considered have been 1) a variation of pH between 6 and 8, since this is the most common range of pH in natural systems, and 2) a range of temperature from 25 to 200 ºC. The LLNL database (using low_albite and the same dolomite as in the WATEQ4F database) has been used to carry out this calculation because the WATEQ4F database was developed to be used up to 100 ºC and at higher temperatures the results should be carefully considered (Ball and Nordstrom, 2001), while temperature range of the LLNL database is up 300 ºC (Johnson et al., 2000).

The most important results are shown in Table 7, Figure 7 and Figure S2 (in the supplementary material; Figure 7 contains the results obtained at pH=6 and the results obtained at pH=7 and pH=8 are in the supplementary material since they are almost the same as those for pH=6). Albitisation and dedolomitisation processes, along with

anhydrite dissolution, are more intense as salinity increases in all the simulations. Dolomite dissolution and calcite precipitation, that is, the dedolomitisation process, is more intense at lower temperatures (Figure 7a and Figure S2a-b) as it was also pointed out by Escorcia et al. (2013). The effect of pH is of minor importance and almost imperceptible in Figure 7a and Figure S2a-b, and while dolomite dissolution is almost the same with the increase of pH, the calcite precipitation is somewhat higher being most important at higher temperatures (Table 7). The dissolution of anhydrite is more intense at low temperatures and it is almost unaffected by the variation of the pH (Figure 7b, Figure S2c-d, Table 7). Finally, the albitisation process displays the opposite behaviour (Table 7, Figure 7c and Figure S2 e-f): the amount of albite precipitated is always the same as the amount of dissolved K-feldspar being more intense at higher temperatures and not affected by the pH variations.

Considering all these results it is clear that halite dissolution and, therefore, the increase of the salinity of the waters, can be a relevant controlling factor for the hydrochemical evolution of the waters. Halite dissolution increases the Na dissolved contents and by the ion-common effect the albitisation process takes place (eq. 2):

$$KAlSi_3O_{8(K-feld)} + Na^+ \rightarrow NaAlSi_3O_{8(alb)} + K^+ \qquad (2)$$

On the other hand, anhydrite solubility is highly influenced by the salinity of the waters due to the salting-in effect (Langmuir, 1997), in the way that the increase in the salinity will lead to a higher solubility of anhydrite (e.g. Li and Duan, 2011; Raines and Dewers, 1997). Therefore, halite dissolution enhances anhydrite dissolution (eq. 3):

$$NaCl_{(hal)} + CaSO_{4(anh)} \rightarrow Na^+ + Cl^- + Ca^{2+}\ SO_4^{2-} \qquad (3)$$

Anhydrite dissolution increases the calcium content of the waters (as shown in eq. 4) and, given that waters are in equilibrium with respect to calcite, the excess of Ca will

produce the oversaturation of calcite and, therefore, its precipitation (common-ion effect; eq. 3):

$$Ca + HCO_3 \rightarrow CaCO_{3(calc)} + H^+ \quad (4)$$

At the same time calcite precipitation leads to a decrease in calcium and HCO_3^- in the solution (eq. 4) and to an increase in the H^+ and the pCO_2 which triggers the dissolution of dolomite (dedolomitisation process; eq. 5):

$$CaMg(CO_3)_{2(dol)} + Ca^{2+} \rightarrow 2CaCO_{3(calc)} + Mg^{2+} \quad (5)$$

This dedolomitisation process, triggered by anhydrite (or gypsum) dissolution, has been reported in other carbonate aquifers, containing dolostones and in contact with anhydrite or gypsum (Appelo and Postma, 2005; Auqué et al., 2009; Back et al., 1983; Capaccioni et al., 2001; Cardenal et al., 1994; Choi et al., 2012; Deike, 1990; Frondini, 2008; Leybourne et al., 2009; López-Chicano et al., 2001; Plummer, 1977; Plummer et al., 1990; Prado-Pérez and Pérez del Villar, 2011; Sacks et al., 1995). However, in the case presented here, although anhydrite dissolution is the direct triggering reaction for the dedolomitisation, the process actually responsible of it is the dissolution of halite. Halite dissolution keeps the dedolomitisation process ongoing even when the waters reach the equilibrium with anhydrite (or gypsum).

Finally, the dissolution of halite also triggers the albitisation process and, although this had previously been identified in diagenetic environments (Egeberg and Aagaard, 1989; Hanor, 1996; Saigal et al., 1988), the results shown in this paper indicate that this process is also feasible in groundwater (thermal) systems at lower temperatures and salinities.

Overall, these results are also relevant for the geological CO_2 storage in saline aquifers or, even, for enhanced geothermal systems (EGS) where saline waters, initially in

equilibrium with the reservoir rocks, are usually involved. The evolution of the dedolomitisation processes has been identified as a critical point in assessing carbonate formations for potential CO_2 storage (e.g. Auqué et al., 2009; Prado-Pérez and Pérez del Villar, 2011 and references therein). And albitisation processes have been identified in CO_2–brine–rock interaction experiments at in situ P–T conditions of the pilot CO_2 storage site at Ketzin in Germany (Fischer et al., 2010) and in the experiments with hydrothermal Na-Cl solutions on fracture surfaces in the geothermal reservoir of the Upper Rhine Graben (Schmidt et al., 2017). Therefore, the evolution and consequences of the processes identified in this paper should be further explored.

5. Conclusions

The spring waters of the Fitero-Arnedillo geothermal system are located in the localities of the same name and separated about 35 km. They are hosted in carbonate-evaporitic materials and they are of chloride-sodium type with near neutral pH and discharge temperature of about 45 ºC. The main differences between these waters are the higher salinity of those emerging in Arnedillo, the slightly higher Ca and Mg contents in Fitero and the calculated reservoir temperature (81 ± 11 ºC in Fitero and 87 ± 13 ºC in Arnedillo). All these together with the mineral equilibria in the reservoir indicate that, although the waters belong to the same geothermal reservoir, they evolve along different flow paths with different intensities of water-rock interaction processes which would justify a more evolved stage of the Arnedillo system compared to the Fitero thermal waters.

Mass-balance and reaction path calculation have been used to assess the main reactions responsible for the chemical differences and evolution of these waters and the results indicate that the triggering process is the halite dissolution, which leads to an albitisation process and to the dissolution of anhydrite, which, in turn, triggers the

calcite precipitation and the dolomite dissolution (dedolomitisation process). The processes identified in this system (dedolomitisation and albitisation) have been identified in different environments under different conditions of temperature, pH and/or salinities, and how these parameters affect them has also been evaluated in this paper. The extension of these processes is higher as the salinity of the waters increases. However, the effect of pH (assessed between 6 and 8) is almost negligible in terms of the mass transfers of the involved phases. Temperature also causes significant variations in a way that the dedolomitisation and anhydrite dissolution are higher at low temperatures and the albitisation is more intense at high temperatures.

These calculations have evidenced the importance that the changes in the salinity of the waters (through halite dissolution) have over the geochemical evolution of waters due to its effect in the water-mineral equilibria attained. Halite dissolution has been proven to trigger a dedolomitisation process even when the waters have reached the equilibrium with respect to anhydrite, calcite and dolomite. Moreover it has been shown that these processes are more general than what was known up to date and deserve future studies, mainly considering their feasibility in particularly relevant situations such as the enhanced geothermal systems and the geological CO_2 storage sites.

6. Acknowledgements

M. Blasco has worked in this study thanks to a scholarship from the Ministry of Science, Innovation and Universities of Spain, for the Training of University Teachers (ref. FPU14/01523). This study forms part of the activities of the Geochemical Modelling Group (University of Zaragoza; Aragón Government).

We are grateful to the staff of the Fitero and Arnedillo spas for their disposition and assistance during the sampling campaign. The technical assistance of Enrique Oliver,

from the Earth Sciences Department of the University of Zaragoza, is acknowledged. The comments from two anonymous reviewers are also appreciated.

7. References

Aagaard, P., Egeberg, P.K., Saigal, G.C., Morad, S., Bjorlykke, K., 1990. Diagenetic albitization of detrital K-feldspar in Jurassic, Lower Cretaceous and Tertiary clastic reservoir rocks from offshore Norway, II. Formation water chemistry and kinetic considerations. J. Sediment. Petrol. 60, 575–581.

Albert, J.F., 1979. Estudio geoquímico preliminar de Navarra, in: II Simposio Nacional de Hidrogeología. Hidrogeología Y Recursos Hidráulicos IV. Sección Quinta: Técnicas Especiales. 22-26 de Octubre de 1979. Pamplona (España), pp. 511–531.

Apollaro, C., Dotsika, E., Marini, L., Barca, D., Bloise, A., de Rosa, R., Doveri, M., Lelli, M., Muto, F., 2012. Chemical and isotopic characterization of the thermomineral water of Terme Sibarite springs (Northern Calabria, Italy). Geochem. J. 46, 117–129.

Appelo, C.A.J., Postma, D., 2005. Geochemistry, Groundwater and Pollution, 2nd ed. ed. A.A. Balkema, Rotterdam.

Arnòrsson, S., Gunnlaugsson, E., Svavarsson, H., 1983. The chemistry of geothermal waters in Iceland. III. Chemical geothermometry in geothermal investigations. Geochim. Cosmochim. Acta 47, 567–577.

Asta, M.P., Gimeno, M.J., Auqué, L.F., Gómez, J., Acero, P., Lapuente, P., 2012. Hydrochemistry and geothermometrical modeling of low-temperature Panticosa geothermal system (Spain). J. Volcanol. Geotherm. Res. 235-236, 84–95.

Asta, M.P., Gimeno, M.J., Auqué, L.F., Gómez, J., Acero, P., Lapuente, P., 2010. Secondary processes determining the pH of alkaline waters in crystalline rock

systems. Chem. Geol. 273, 41–52.

Auqué, L.F., Acero, P., Gimeno, M.J., Gómez, J.B., Asta, M.P., 2009. Hydrogeochemical modeling of a thermal system and lessons learned for CO2 geologic storage. Chem. Geol. 268, 324–336.

Auqué, L.F., Fernández, J., Tena Calvo, J.M., 1988. Las aguas termaldes de Fitero (Navarra) y Arnedillo (Rioja). I. Análisis geoquímico de los estados de equilibrio-desequilibrio en las surgencias. Estud. geológicos 44, 285–292.

Auqué, L.F., Mandado, J., López, P.L., Lapuente, P.L., Gimeno, M.J., 1998. Los sistemas geoterhmales del Pirineo Central. III. Evaluación de las condiciones en profundidad y evolución de las soluciones hidrotermales durante su ascenso. Estud. geológicos 54, 25–37.

Auqué, L.F., Mandado, J., López, P.L., Lapuente, P.L., Gimeno, M.J., 1997. Los sistemas geotermales del Pirineo Central. II. Resultados de la aplicación de técnicas geotermométricas. Estud. geológicos 53, 45–54.

Awaleh, M.O., Hoch, F.B., Boschetti, T., Soubaneh, Y.D., Egueh, N.M., Elmi, S.K., Mohamed, J., Khaireh, M.A., 2015. The geotermal resources of the Republic of Djibouti – II: Geochemical study of the Lake Abhe geothermal field. J. Geochemical Explor. 159, 129–147.

Back, W., Hanshaw, B.B., Plummer, L.N., Rahn, P.H., Rightmire, C.T., Rubin, M., 1983. Process and rate of dedolomitization: mass transfer and 14C dating in a regional carbonate aquifer. Geol. Soc. Am. Bull. 94, 1415–1429.

Ball, J.W., Nordstrom, D., 2001. User's manual for WATEQ4F with revised thermodynamic database and test cases for calculating speciation of major, trace and redox elements in natural waters, in: U.S. Geological Survey (Ed.), Water-

Resources Investigation Report. U.S. Geological Survey, Menlo Park (California), pp. 91–183.

Bischoff, J.L., Juliá, R., Shanks III, W.C., Rosenbauer, R.J., 1994. Karstification without carbonic-acid: bedrock dissolution by gypsum-driven dedolomitization. Geology 22, 995–998.

Blasco, M., Auqué, L.F., Gimeno, M.J., Acero, P., Asta, M.P., 2017. Geochemistry, geothermometry and influence of the concentration of mobile elements in the chemical characteristics of carbonate-evaporitic thermal systems. The case of the Tiermas geothermal system (Spain). Chem. Geol. 466, 696–709.

Blasco, M., Gimeno, M.J., Auqué, L.F., 2018. Low temperature geothermal systems in carbonate-evaporitic rocks: Mineral equilibria assumptions and geothermometrical calculations. Insights from the Arnedillo thermal waters (Spain). Sci. Total Environ. 615, 526–539. doi:10.1016/j.scitotenv.2017.09.269

Boschetti, T., 2013. Oxygen isotope equilibrium in sulfate-water systems: A revisión of geothermometric applications in low-enthalpy systems. J. Goechemical Explor. 124, 92–100.

Boschetti, T., Cortecci, G., Toscani, L., Iacumin, P., 2011. Sulfur and oxygen isotope compositions of Upper Triassic sulfates from northern Apennines (Italy): paleogeographic and hydrogeochemical implications. Geol. Acta 9, 129–147.

Budai, J.M., Lohmann, K.C., Owen, R.M., 1984. Burial dedolomite in the Mississippian Madison Limestone, Wyoming and Utah Thrust Belt (USA). J. Sediment. Petrol. 54, 276–288.

Buil, B., Gómez, P., Turrero, M.J., Garralón, A., Lago, M., Arranz, E., de la Cruz, B., 2006. Factors that control the geochemical evolution of hydrothermal systems of

alkaline water in granites in Central Pyrenees (Spain). J. Iber. Geol. 32, 283–302.

Busby, J.F., Plummer, L.N., Lee, R.W., Hanshaw, B.B., 1991. Geochemical Evolution of Water in the Madison Aquifer in Parts of Montana, South Dakota, and Wyoming, in: U.S. Geological Survey Professional Paper 1273-F. United States Government Printing Office, Washington, p. 89.

Cañaveras, J.C., Sánchez-Moral, S., Calvo, J.P., Hoyos, M., Ordóñez, S., 1996. Dedolomites associated with karstification. An example of early dedolomitization in lacustrine sequences from the Tertiary Madrid Basin, Central Spain. Carbonates Evaporites 11, 85–103.

Capaccioni, B., Didero, M., Paletta, C., Salvadori, P., 2001. Hydrogeochemistry of groundwaters from carbonate formations with basal gypsiferous layers: an example from the Mt Catria Mt Nerone ridge (Northern Appennnines, Italy). J. Hydrol. 253, 14–26.

Cardenal, J., Benavente, J., Cruz-Sanjulián, J.J., 1994. Chemical evolution of groundwater in triassic gypsum-bearing carbonate aquifers (Las Alpujarras, southern Spain). J. Hydrol. 161, 3–30.

Chiodini, G., Frondini, F., Marini, L., 1995. Theoretical geothermometers and pCO2 indicators for aqueous solutions coming from hydrothermal systems of medium-low temperature hosted in carbonate-evaporite rocks. Application to the thermal springs of the Etruscan Swell. Italy. Appl. Geochemistry 10, 337–346.

Choi, B.Y., Yun, S.T., Mayer, B., Hong, S.Y., Kim, K.H., Jo, H.Y., 2012. Hydrogeochemical processes in clastic sedimentary rocks, South Korea: a natural analogue study of the role of dedolomitization in geologic carbon storage. Chem. Geol. 306-307, 103–113.

Choi, H.S., Koh, Y.K., Bae, D.K., Park, S.S., Hutcheon, I., Yun, S.T., 2005. Estimation of deep-reservoir temperature of CO2-rich springs in Kangwon district, South Korea. J. Volcanol. Geotherm. Res. 141, 77–89.

Clark, I., Fritz, P., 1997. Environmental Isotopes in Hydrogeology. CRC Press/Lewis Publishers, Boca -Raton (Florida).

Coloma, P., 1998. El agua subterránea en La Rioja. Zubía Monográfico 10, 63–132.

Coloma, P., Sánchez, J.A., Jorge, J.C., 1998. Simulación matemática del flujo y transporte de calor del sector oriental de la Cuenca de Cameros. Zubía Monográfico 10, 45–61.

Coloma, P., Sánchez, J.A., Martínez, F.J., 1997a. Sistemas de flujo subterráneo regional en el acuífero carbonatado mesozoico de la Sierra de Cameros. Sector Oriental. Estud. geológicos 53, 159–172.

Coloma, P., Sánchez, J.A., Martínez, F.J., 1996. Procesos geotérmicos causados por la circulación del agua subterránea en el contacto entre la Sierra de Cameros y la Depresión Terciaria del Ebro. Geogaceta 20, 749–753.

Coloma, P., Sánchez, J.A., Martínez, F.J., 1995. El drenaje subterráneo de la cordillera Ibércia en la depresión terciaria del Ebro (sector Riojano). Geogaceta 17, 68–71.

Coloma, P., Sánchez, J.A., Martínez, F.J., Pérez, A., 1997b. El drenaje subterráneo de la Cordillera Ibérica en la Depresión terciaria del Ebro. Rev. la Soc. Geológica España 10, 205–218.

Craig, H., 1961. Isotopic variations in meteoric waters. Science (80-.). 133, 1702–1703.

D´Amore, F., Fancelli, R., Caboi, R., 1987. Observations of the application of chemical geothermometers to some hydrothermal systems in Sardinia. Geothermics 16, 271–

282.

Deike, R.G., 1990. Dolomite dissolution rates and possible Holocene dedolomitization of water-bearing units in the Edwards aquifer, south-central Texas. J. Hydrol. 112, 335–373.

Dias Lima, R., De Ros, L.F., 2002. The role of depositional setting and diagenesis on the reservoir quality of Devonian sandsones from Solimoes Basin, Brazilian Amazonia. Mar. Pet. Geol. 19, 1047–1071.

Díaz-Teijeiro, M.F., Rodríguez-Arévalo, J., Castaño, S., 2009. La Red Española de Vigilancia de Isótopos en la Precipitación (REVIP): distribución isotópica espacial y aportación al conocimiento del ciclo hidrológico. Ing. Civ. 155, 87–97.

Egeberg, P.K., Aagaard, P., 1989. Origin and evolution of formation waters from oil fields on the Norwegian shelf. Appl. Geochemistry 4, 131–142.

Escorcia, L.C., Gomez-Rivas, E., Daniele, L., Corbella, M., 2013. Dedolomitization and reservoir quality: Insights from reactive transport modelling. Geofluids 13, 221–231. doi:10.1111/gfl.12023

Fernández, J., Auqué, L.F., Sánchez Cela, V.S., Guaras, B., 1988. Las aguas termales de Fitero (Navarra) y Arnedillo (Rioja). II. Análisis comparativo de la aplicación de técnicas geotermométricas químicas a aguas relacionadas con reservorios carbonatado-evaporíticos. Estud. geológicos 44, 453–469.

Fischer, S., Liebscher, A., Wandrey, M., 2010. CO2-brine-rock interaction - First results of long-term exposure experiments at in situ P-T conditions of the Ketzin CO2reservoir. Chemie der Erde 70, 155–164.

Fouillac, C., Michard, G., 1981. Sodium/lithium ratio in water applied to geothermometry of geothermal reservoirs. Geothermics 10, 55–70.

Fournier, R.O., 1982. Water geothermometers applied to geothermal energy, in: D'Amore, F. (Ed.), Applications of Geochemistry in Geothermal Reservoir Development. UNITAR/UNDO centre on Small Energy Resources, Rome, Italy, Italy, pp. 37–69.

Fournier, R.O., 1981. Application of water geochemistry to geothermal exploration and reservoir engineering, in: L, R., L.J.P., M. (Eds.), Geothermal Systems: Principles and Case Histories. John Willey & Sons Ltd., New York, pp. 109–141.

Fournier, R.O., 1977. Chemical geothermometers and mixing models for geothermal systems. Geothermics 5, 41–50.

Fournier, R.O., Truesdell, A.H., 1973. An empirical Na–K–Ca geothermometer for natural waters. Geochim. Cosmochim. Acta 37, 1255–1275.

Friedman, I., O'Neil, J.R., 1977. Compilation of stable isotope fractionation factors of geochemical interest, in: Fleischer, M. (Ed.), Data on Geochemistry, USGS Proffesional Paper 440-KK. United States Government Printing Office, Washington, p. 109.

Frondini, F., 2008. Geochemistry of regional aquifers hosted by carbonate-evaporite formations in Umbria and southern Tuscany (central Italy). Appl. Geochemistry 23, 2091–2104.

Giggenbach, W.F., 1988. Geothermal solute equilibria. Derivation of Na-K-Mg-Ca geoindicators. Geochim. Cosmochim. Acta 52, 2749–2765.

Giggenbach, W.F., Gonfiantini, R., Jangi, B.L., Truesdell, A.H., 1983. Isotopic and chemical composition of Parbati valley geothermal discharges, N.W. Himalaya. India. Geothermics 12, 199–222.

Gil, A., Villalaín, J.J., Barbero, L., González, G., Mata, P., Casas, A.M., 2002.

Aplicación de Técnicas geoquímicas, geofísicas y mineralógicas al estudio de la Cuenca de Cameros. Implicaciones geométricas y evolutivas. Zubía Monográfico 14, 65–98.

Gil, J., Carenas, B., Segura, M., García-Hidalgo, J.F., García, A., 2004. Revisión y correlación de las unidades litoestratigráficas del Cretácico Superior en la región central y oriental de España. Rev. la Soc. Geológica España 17, 249–266.

Gökgöz, A., Tarkan, G., 2006. Mineral equilibria and geothermometry of the Dalaman–Köycegiz thermal springs, southern Turkey. Appl. Geochemistry 21, 253–268.

Goy, A., Gómez, J.J., Yébenes, A., 1976. El Jurásico de la Rama Castellana de la Cordillera Ibérica (Mitad norte) I. Unidades litoestratigráficas. Estud. geológicos 32, 391–423.

Gutiérrez, P., 1801. Descripción de los Reales Baños de Arnedillo y análisis de sus aguas. Imprenta Fermín Villalpando, Madrid.

Halas, S., Pluta, I., 2000. Empirical calibration of isotope thermometer δ18O (SO42−)–δ18O (H2O) for low temperature brines, in: V Isotope Workshop. European Society for Isotope Research, Kraków, Poland, pp. 68–71.

Hanor, J.S., 1996. Variations in chloride as a drving force in siliciclastic diagensis. Siliciclastic Diagenes. Fluid Flow Concepts Appl. SEPM Spec. Publ. 55, 3–12.

Hanshaw, B.B., Back, W., 1985. Deciphering hydrological systems by means of geochemical processes. Hydological Sci. J. 30, 257–271.

Jacobson, A.D., Wasserburg, G.J., 2005. Anhydrite and the Sr isotope evolution of groundwater in a carbonate aquifer. Chem. Geol. 214, 331–350.

Johnson, J., Anderson, G., Parkhurst, D., 2000. Database “thermo.com.V8.R6.230,”

Rev. 1.11. Livermore, California.

Kharaka, Y.K., Mariner, R.H., 1989. Chemical geothermometers and their application to formation waters from sedimentary basins, in: Naeser, N.D., McCollon, T.H. (Eds.), Thermal History of Sedimentary Basins. Springer, Berlin, pp. 99–117.

Langmuir, D., 1997. Aqueous environmental geochemistry. Prentice Hall, Upper Saddle River, New Jersey.

Leybourne, M.I., Betcher, R.N., McRitchie, W.D., Kaszycki, C.A., Boyle, D.R., 2009. Geochemistry and stable isotopic composition of tufa waters and precipitates from the Interlake Region, Manitoba. Chem. Geol. 260, 221–233.

Li, J., Duan, Z., 2011. A thermodynamic model for the prediction of phase equilibria and speciation in the H2O–CO2–NaCl–CaCO3–CaSO4 system from 0 to 250 _C, 1 to 1000 bar with NaCl concentrations up to halite saturation. Geochim. Cosmochim. Acta 75, 4351–4376.

López-Chicano, M., Bouamama, M., Vallejos, A., Pulido-Bosch, A., 2001. Factors which determine the hydrogeochemical behaviour of karstic springs. A case study from the Betic Cordilleras, Spain. Appl. Geochemistry 16, 1179–1192.

Mariner, R.H., Evans, W.C., Young, H.W., 2006. Comparison of circulation times of thermal waters discharging from the Idaho batholith based on geothermometer temperatures, helium concentrations, and 14C measurements. Geothermics 35, 3–25.

Marini, L., 2004. Geochemical techniques for the exploration and exploitation of geothermal energy. Laboratorio di Geochimica, Università degli Studi di Genova, Genova.

Mas, J.R., Alonso, A., Guimera, J., 1993. Evolución tectonosedimentaria de una cuenca

extensional intraplaca: la cuenca finijurásica-eocretácica de los Cameros (La Rioja-Soria). Rev. la Soc. Geológica España 6, 129–144.

Mezquíriz, M.A., 2004. Las termas romanas de Fitero. Trab. Arqueol. Navarra 17, 273–286.

Michard, G., 1983. Recueil de donnés thermodynamiques concernant les équilibres eaux-minéraux dans les réservoirs géothermaux. Commission des Communautés Europeennes, Luxembourg.

Michard, G., 1979. Gothermométres chimiques. Bur. Rech. Géologiques Minières (2nd Ser.), Sect. III 2, 183–189.

Michard, G., Bastide, J.P., 1988. Géochimie de la nappe du Dogger du Bassin de Paris. J. Volcanol. Geotherm. Res. 35, 151–163.

Michard, G., Grimaud, D., D'Amore, F., Fancelli, R., 1989. Influence of mobile ion concentration on the chemical composition of geothermal waters in granitic areas. Example of hot springs from Piemonte (Italy). Geothermics 18, 729–741.

Michard, G., Roekens, E., 1983. Modelling of the chemical composition of alkaline hot waters. Geothermics 12, 161–169.

Michard, G., Sanjuan, B., Criaud, A., Fouillac, C., Pentcheva, E.N., Petrov, P.S., Alexieva, R., 1986. Equilibria and geothermometry in hot alkaline waters from granites of S.W. Bulgaria. Geochem. J. 20, 159–171.

Mohammadi, Z., Bagheri, R., Jahanshahi, R., 2010. Hydrogeochemistry and geothermometry of Changal thermal springs, Zagros region, Iran. Geothermics 39, 242–249.

Moral, F., Cruz-Sanjulián, J.J., Olías, M., 2008. Geochemical evolution of groundwater

in the carbonate aquifers of Sierra de Segura (Betic Cordillera, southern Spain). J. Hydrol. 360, 281–296.

Mutlu, H., Güleç, N., 1998. Hydrogeochemical outline of thermal waters and geothermometry applications in Anatolia (Turkey). J. Volcanol. Geotherm. Res. 85, 495–515.

Palandri, J.L., Reed, M.H., 2001. Reconstruction of in situ composition of sedimentary formation waters. Geochim. Cosmochim. Acta 65, 1741–1767.

Pang, Z., Reed, M.H., 1998. Theoretical chemical thermometry on geothermal waters: Problems and methods. Geochim. Cosmochim. Acta 62.

Parkhurst, D.L., Appelo, C.A.J., 2013. Description of Input and Examples for PHREEQC Version 3. A Computer Program for Speciation, Batch Reaction, One Dimensional Transport, and Inverse Geochemical Calculations, in: U.S. Geological Survey (Ed.), Techniques and Methods, Book 6, Chap. A43. U.S. Geological Survey, Denver, Colorado.

Pastorelli, S., Marini, L., Hunziker, J.C., 1999. Water chemistry and isotope composition of the Acquarossa thermal system, Ticino, Switzerland. Geothermics 28, 75–93.

Plummer, L.N., 1977. Defining reactions and mass transfer in part of the Floridan aquifer. Water Resour. Res. 13, 801–812.

Plummer, L.N., Back, W., 1980. The mass balance approach: application to interpreting the chemical evolution of hydrologic systems. Am. J. Sci. 280, 130–142.

Plummer, L.N., Busby, J.F., Lee, R.W., Hanshaw, B.B., 1990. Geochemical modelling of the Madison aquifer in parts of Montana, Wyoming, and South-Dakota. Water Resour. Res. 26, 1981–2014.

Plummer, L.N., Parkhurst, D.L., Thorstenson, D.C., 1983. Development of reaction models for ground-water systems. Geochim. Cosmochim. Acta 47, 665–686.

Prado-Pérez, A.J., Pérez del Villar, L., 2011. Dedolomitization as an analogue process for assessing the long-term behaviour of a CO 2 deep geological storage: The Alicún de las Torres thermal system (Betic Cordillera, Spain). Chem. Geol. 289, 98–113. doi:10.1016/j.chemgeo.2011.07.017

Raines, M.A., Dewers, T.A., 1997. Dedolomitization as a driving mechanism for kars generation in Permian blaine Formation, southwestern Oklahoma, USA. Carbonates and Evaporites 12, 24–31.

Román-Mas, A., Lee, R.W., 1987. Geochemical evolution of waters within the North Coast limestone aquifers of Puerto Rico: a concepualization based on a flow path in the Barceloneta area, in: U.S. Geological Survey Water-Resources Investigaions Report 86-4080. U.S. Geological Survey, San Juan, Puerto Rico, p. 28.

Sacks, L.A., Herman, J.S., Kauffman, S.J., 1995. Controls on high sulfate concentrations in the upper Floridan aquifer in southwest Florida. Water Resour. Res. 31, 2541–2551.

Saigal, G.C., Sadoon, M., Bjorlykke, K., Egeberg, P.K., Aagaard, P., 1988. Diagenetic albitization of detrital K-feldspar in Jurassic, Lower Cretaceous and Tertiay clastic reservoir rocks from offshore Norway, I. Textures and origin. J. Sediment. Petrol. 58, 1003–1013.

Sánchez, J.A., Coloma, P., 1998. Hidrogeología de los manantiales termales de Arnedillo. Zubía Monográfico 10, 11–25.

Sánchez, J.A., Coloma, P., Pérez, A., 1999. Sedimentary processes related to the groundwater flows from the Mesozoic Carbonate Aquifer of the Iberian Chain in

the Tertiary Ebro Basin, northeast Spain. Sediment. Geol. 129, 201–213.

Schmidt, R.B., Bucher, K., Drüppel, K., Stober, I., 2017. Experimental interaction of hydrothermal Na-Cl solution with fracture surfaces of geothermal reservoir sandstone of the Upper Rhine Graben. Appl. Geochemistry 81, 36–52.

Seal, R.R.I., Alpers, C.N., Rye, R.O., 2000. Stable isotope systematics of sulfate minerals, in: Alpers, C.N., Jambor, J.L., Nordstrom, D.. (Eds.), Sulfate Minerals — Crystallography: Geochemistry and Environmental Significance. Mineral Society of America, Chantilly (Virginia), pp. 541–602.

Spycher, N., Peiffer, L., Sonnenthal, E.L., Saldi, G., Reed, M.H., Kennedy, B.M., 2014. Integrated multicomponent solute geothermometry. Geothermics 51, 113–123.

Stefánsson, A., Arnórsson, S., 2000. Feldspar saturation state in natural waters. Geochim. Cosmochim. Acta 64, 2567–2584.

Stoessell, R.K., Klimentidis, R.E., Prezbindoski, D.R., 1987. Dedolomitization in Na-Cl-Ca brines from 100ºC to 200ºC at 300 bar. Geochim. Cosmochim. Acta1 51, 847–855.

Truesdell, A.H., 1976. Geochemical Techniques in Exploration. Summary of Section III, in: Proceedings of the Second United Nations Symposium on the Development Y Use of Geothermal Resources. San Francisco (California), pp. iii–xxix.

Verma, S.P., Santoyo, E., 1997. New improved equations for Na/K, Na/Li and SiO2 geothermometers by outlier detection and rejection. J. Volcanol. Geotherm. Res. 79, 9–24.

Wang, J., Jin, M., Jia, B., Kang, F., 2015. Hydrochemical characteristics and geothermometry applications of thermal groundwater in northern Jinan, Shandong, China. Geothermics 57, 185–195.

Woo, K.S., Moore, C.H., 1996. Burial dolomitization and dedolomitization of the late Cambrian Wagok Formation, Yeongweol, Korea. Carbonates and Evaporites 11, 104–112.

Zeebe, R.E., 2010. A new value for the stable oxygen isotope fractionation between dissolved sulfate ion and water. Geochim. Cosmochim. Acta 74, 818–828.

Zhu, C., Anderson, G., 2002. Environmental Applications of Geochemical Modeling. Cambridge University Press.

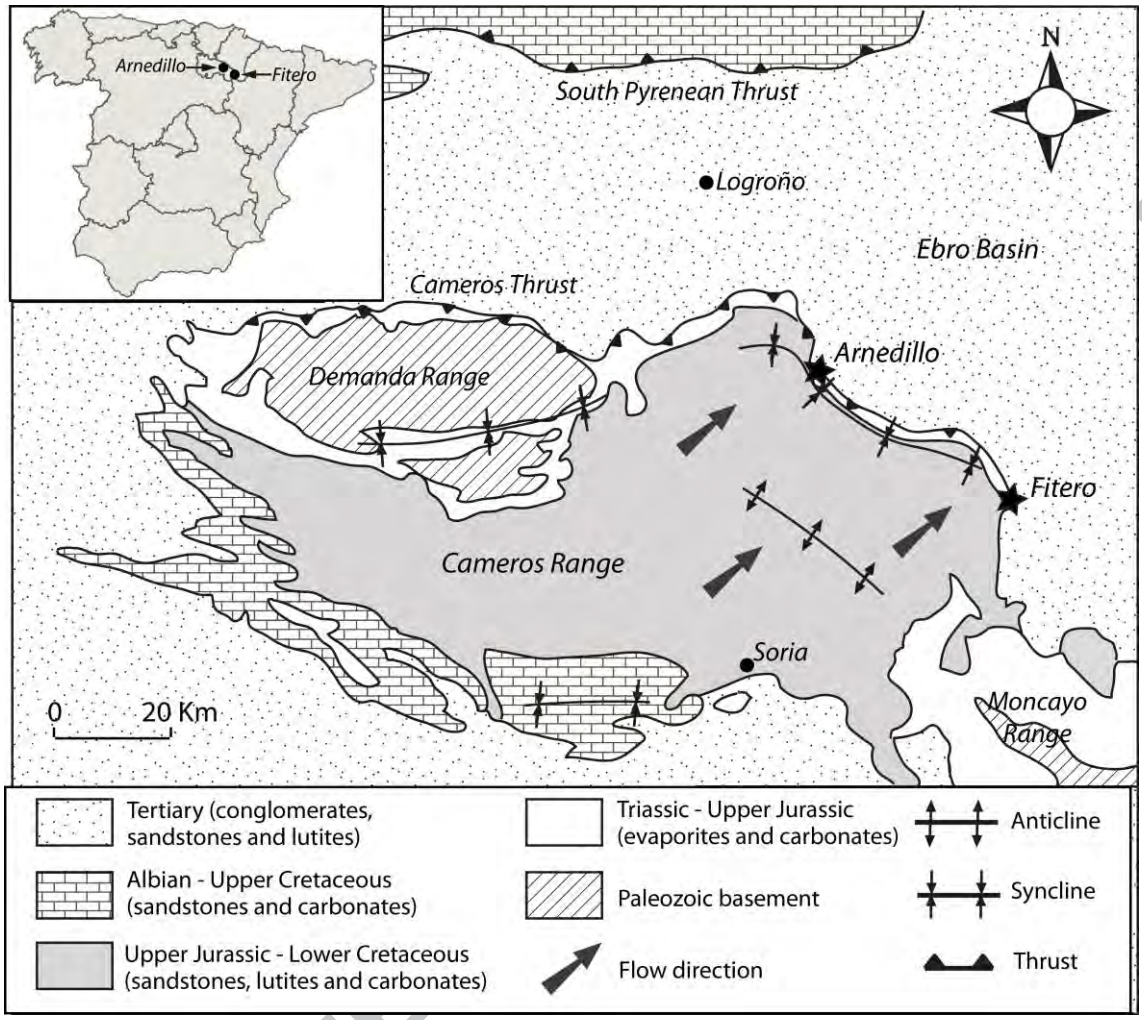
Arnedillo
Fitero
South Pyrenean Thrust
N
Logroño
Ebro Basin
Cameros Thrust
Demanda Range
Arnedillo
Fitero
Cameros Range
Soria
Moncayo Range
0
20 Km
Tertiary (conglomerates, sandstones and lutites)
Albian - Upper Cretaceous (sandstones and carbonates)
Upper Jurassic - Lower Cretaceous (sandstones, lutites and carbonates)
Triassic - Upper Jurassic (evaporites and carbonates)
Paleozoic basement
Flow direction
Anticline
Syncline
Thrust

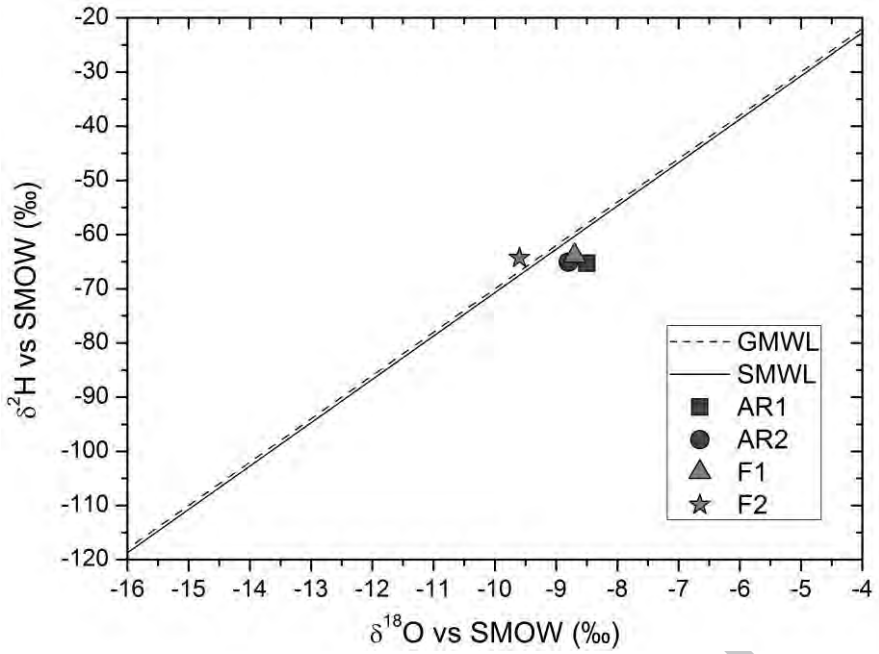

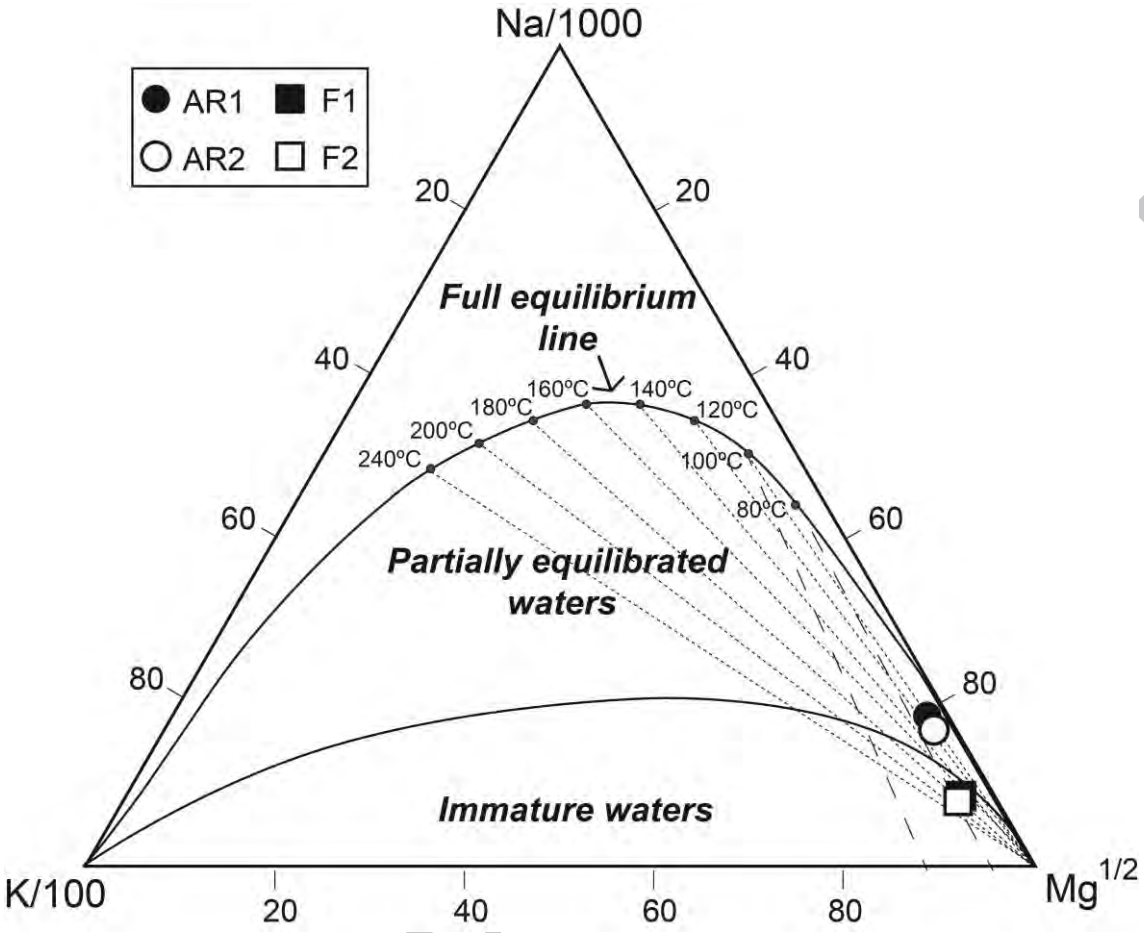
Na/1000
AR1
F1
AR2
F2
20
20
Full equilibrium line
40
40
160°C
140°C
180°C
120°C
200°C
240°C
100°C
80°C
60
60
Partially equilibrated waters
80
80
Immature waters
K/100
20
40
60
80
Mg1/2

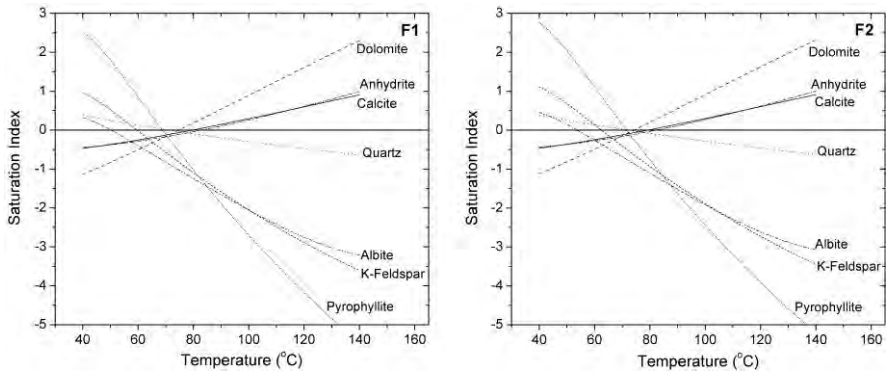

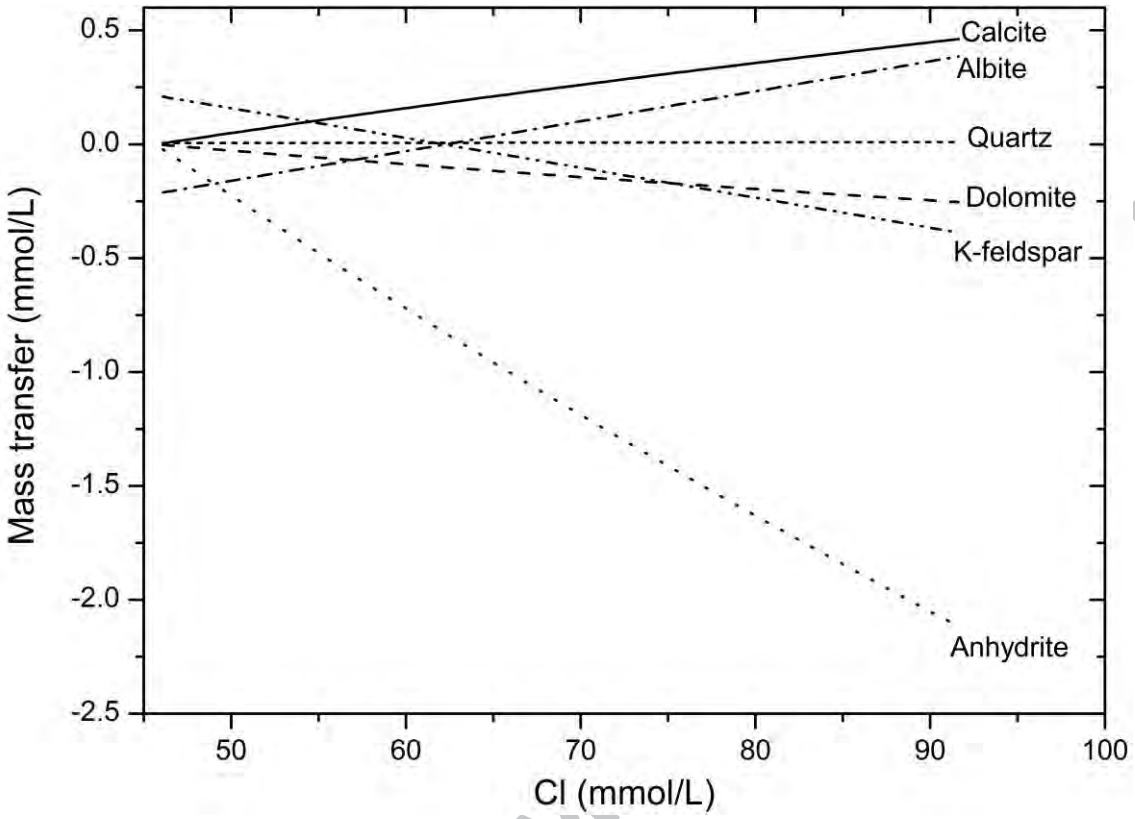

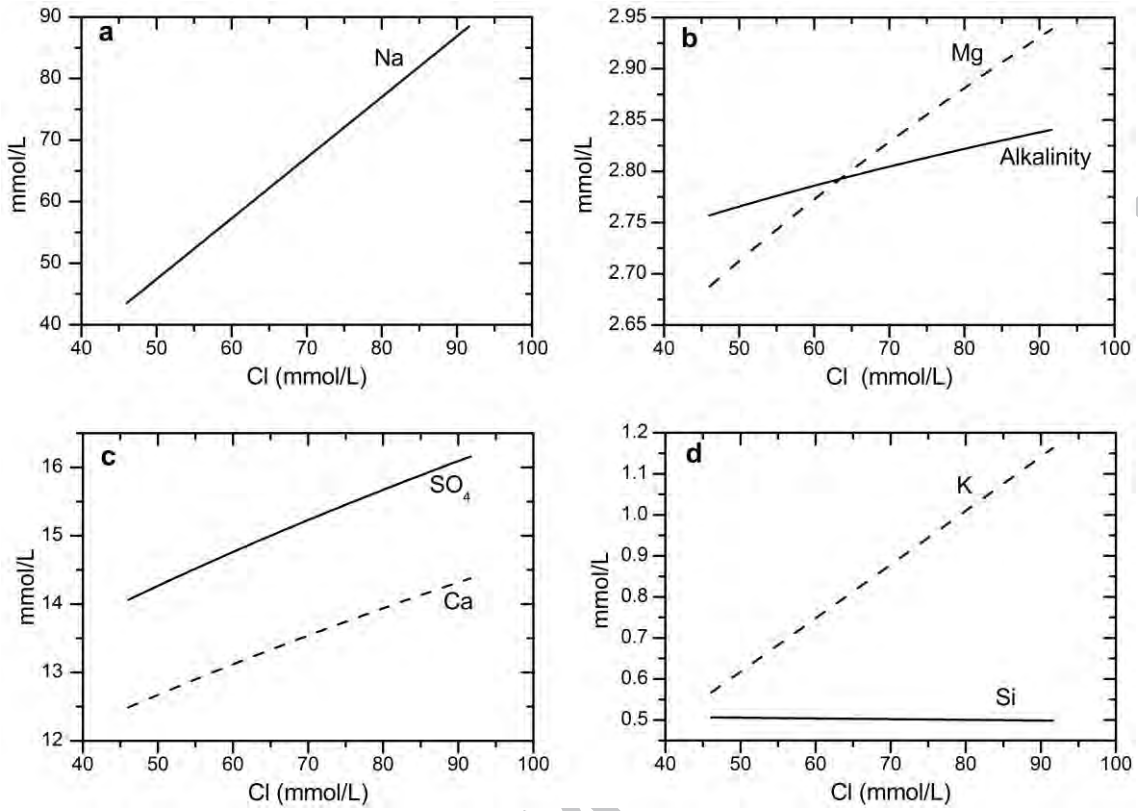

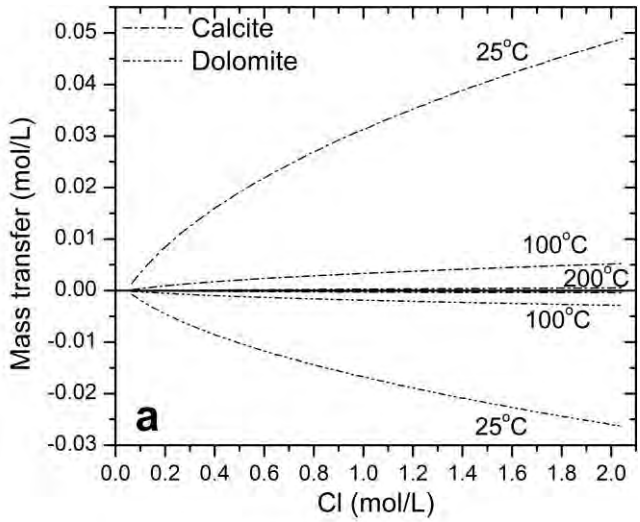

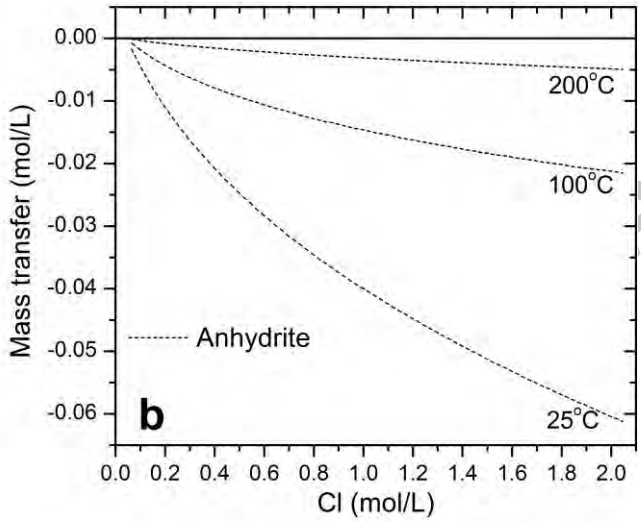

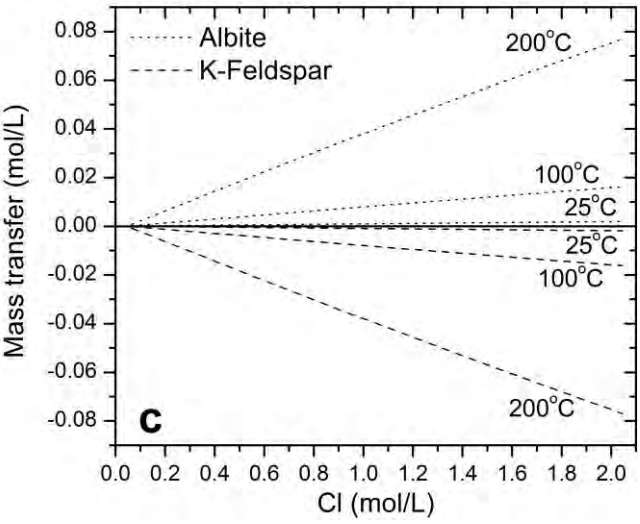

Figure 1. Location of the Arnedillo and the Fitero geothermal springs and geological map of the area (modified form Blasco et al. 2018).

Figure 2. $\delta^{2}H$ – $\delta^{18}O$ diagram showing the isotopic composition of the samples from Arnedillo and Fitero. The Global Meteoric Water Line (GMWL) and the Spanish Meteoric Water Line (SMWL) are also shown.

Figure 3. Location of the Fitero and Arnedillo samples in the Giggenbach diagram. The dotted line is calculated with the Na-K Fournier (1979) calibrate and with the Giggenbach (1988) one for Mg-K; the solid line is calculated with Na-K and Mg-K calibrates of Giggenbach (1988).

Figure 4. Evolution with temperature of the saturation indices of the different mineral supposed to be in equilibrium with the water of the Fitero samples. These results were obtained after the theoretical reconstruction of the waters at depth by adding CO_2 to compensate the CO_2 outgassing during the ascent of the waters.

Figure 5. Mass transfers of the different mineral phases when the water of the Fitero sample, with Cl^- = 45.6 mmol/L, dissolves 46 mmol/L of halite (represented by the increase in the Cl^- concentration) Negative and positive slopes indicate dissolution and precipitation, respectively.

Figure 6. Changes in the elemental contents in the Fitero waters, with Cl^- = 45.6 mmol/L, when 46 mmol/L of halite are dissolved (represented by the increase in the Cl^- concentration).

Figure 7. Evolution with the increase of salinity (dissolution of halite) at different temperatures (25, 100 and 200 ºC) and a pH = 6, of a) calcite precipitation and dolomite dissolution (dedolomitisation process); b) anhydrite dissolution; and c) albite precipitation and K-feldspar dissolution (albitisation process).

Table 1. Chemical and isotopic data of the thermal waters included in this study. TDS (calculated using PHREEQC) and dissolved elements are expressed in ppm. The molar ratios are also shown, the $Ca+Mg/HCO_3+SO_4$ is in eq/L.

	AR1	AR2	F1	F2
Temp. (°C)	45.30	39.50	45.50	45.10
TDS	7720.9	7352.1	4820.2	4854.7
pH	6.87	7.05	6.86	7.11
HCO_3^-	179.88	181.58	174.02	175.36
Cl^-	3220.00	3030.00	1610	1620
SO_4^-	1541.00	1537.00	1376	1401
Ca	444.00	443.00	469	476
Mg	75.50	73.80	92.10	94.60
Na	2099.00	1941.00	981	982
K	20.60	22.90	30.20	31.80
Sr	9.90	9.80	11.10	11.20
F	2.36	2.30	0.992	1.02
Al	0.0142	0.0643	0.0059	0.0075
Li	0.2901	0.2708	0.4755	0.4836
SiO_2	30.87	29.10	23.75	24.39
$\delta^{18}O$ vs. SMOW in (H_2O)	-8.5	-8.8	-8.7	-9.6
$\delta^{2}H$ vs. SMOW (H_2O)	-65.3	-65.1	-63.9	-64.3
$\delta^{18}O$ vs. SMOW in (SO_4^{2-})	14.1	14	14.2	13.9
$\delta^{34}S$ vs. CDT (in SO_4^{2-})	14.8	14.8	14.9	14.9
$\delta^{13}C$ vs. PDB (in CO_2)	-4.16	-5.52	-8.42	-8.1
Na/Cl	1.01	0.99	0.94	0.93
Ca/SO_4	0.69	0.69	0.82	0.81
$Ca+Mg/HCO_3+SO_4$	0.81	0.81	0.98	0.98
Ca/HCO_3	3.76	3.71	4.10	4.13
$Ca+Mg/HCO_3$	4.81	4.73	5.43	5.49
Mg/Ca	0.27	0.28	0.32	0.33
% imbalance	-2.41	-3.28	-1.7	-1.8

Table 2. Saturation state of the waters with respect to different mineral phases.

	AR1	AR2	F1	F2
Log pCO2(g)	-1.59	-1.81	-1.58	-1.84
Calcite	0.08	0.20	0.14	0.39
Dolomite	-0.29	0.13	0.14	0.64
Anhydrite	-0.48	-0.50	-0.41	-0.40
Gypsum	-0.37	-0.36	-0.31	-0.30
Fluorite	-0.31	-0.27	-0.98	-0.95
Halite	-3.96	-4.01	-4.56	-4.56
Quartz	0.57	0.63	0.31	0.32
Chalcedony	0.30	0.35	0.03	0.05
Albite	1.84	2.73	0.36	0.53
K-Feldspar	1.91	2.95	0.93	1.13
Kaolinite	4.04	5.57	2.79	2.58
Pyrophyllite	3.22	4.81	1.43	1.25
Laumontite	1.18	2.81	-0.54	-0.24

Table 3. Temperatures (ºC) obtained with different chemical and isotopic geothermometers and calibrates for the Arnedillo and Fitero samples.

Geothemometer	Calibrate	AR1	AR2	F1	F2
SiO_2-quartz	Truesdell, 1976	81	78	70	71
	Fournier (1977)	80	78	70	71
	Michard (1979)	82	80	71	72
SiO_2-chalcedony	Fournier (1977)	49	47	38	40
	Arnòrsson et al. (1983)	52	50	42	43
Na-K	Giggenbach (1988)	97	105	153	160
	Fournier (1979)	75	84	133	136
	Verma and Santoyo (1997)	83	91	139	142
K-Mg	Giggenbach et al. (1983)	61	64	67	68
Na-K-Ca	Fournier and Truesdell (1973)	88	91	91	92
Ca-Mg	Chiodini et al. (1995)	116	117	108	107
SO_4-F	Chiodini et al. (1995)	-10	-11	-36	-35
SO_4-H_2O ($\delta^{18}O_{HSO4-H2O}$)	Seal et al. (2000)[1]	66	64	64	60
	Friedman and O'Neil (1977)	69	68	66	64
SO_4-H_2O ($\delta^{18}O_{SO4-H2O}$)	Halas and Pluta (2000)	18	17	17	14
	Zeebe (2010)	25	25	24	21
SO_4-H_2O ($\delta^{18}O_{CaSO4-H2O}$)	Boschetti et al. (2011)[2]	75	74	73	70

[1]This calibrate is the combination of those of Lloyd (1968) and Mizutani and Rafter (1969).

[2]This calibrate is the combination of those of Chiba et al. (1981) and Zheng (1999).

Table 4. Temperatures (°C) at which the different mineral phases considered converge towards equilibrium in the geothermometrical modelling for the Fitero and Arnedillo samples.

Mineral phase	F1	F2	AR1	AR2
Calcite	79	79	91	92
Dolomite	74	74	83	83
Quartz	71	72	97	94
Anhydrite	82	82	88	87
Albite	50	53	85	99
K-feldspar	60	62	78	91
Pyrophyllite	60	71	91	107

Table 5. Different models obtained in the mass balance calculation between samples F1 and AR1 as initial and final solutions, respectively. The mass transfer of the mineral phases and the cationic exchanges are given in mmol/L (negative means precipitation whilst positive means dissolution). The models selected as most plausible are highlighted in grey.

Model	Halite	Calcite	Anhydrite	Dolomite	Quartz	Albite	K-feldspar	NaX	CaX_2	MgX_2
1	44.51	0.00	1.38	0.04	0.07	-0.56	0.56	5.97	-2.39	-0.59
2	44.51	0.00	1.38	0.02	0.00	-0.54	0.56	5.95	-2.40	-0.57
3	44.51	1.19	1.38	-0.55	0.07	-0.56	0.56	5.97	-2.99	0.00
4	44.51	1.14	1.38	-0.55	0.00	-0.54	0.56	5.95	-2.97	0.00
5	44.51	-4.78	1.38	2.43	0.07	-0.56	0.56	5.97	0.00	-2.99
6	44.51	-4.74	1.38	2.39	0.00	-0.54	0.56	5.95	0.00	-2.97
7	44.51	0.00	1.38	0.02	0.00	-0.54	0.56	5.95	-2.40	-0.57
8	44.51	0.09	1.38	0.00	0.07	-0.56	0.56	5.97	-2.43	-0.55
9	44.51	0.04	1.38	0.00	0.00	-0.54	0.56	5.95	-2.39	-0.58
10	44.51	0.00	1.38	0.04	0.07	-0.56	0.56	5.97	-2.39	-0.59
11	44.51	1.14	1.38	-0.55	0.00	-0.54	0.56	5.95	-2.97	0.00
12	44.51	-4.74	1.38	2.39	0.00	-0.54	0.56	5.95	0.00	-2.97
13	44.51	0.04	1.38	0.00	0.00	-0.54	0.56	5.95	-2.39	-0.58
14	44.51	1.19	1.38	-0.55	0.07	-0.56	0.56	5.97	-2.99	0.00
15	44.51	-4.78	1.38	2.43	0.07	-0.56	0.56	5.97	0.00	-2.99
16	44.51	0.09	1.38	0.00	0.07	-0.56	0.56	5.97	-2.43	-0.55

Table 6. Results obtained in the reaction-path calculation. The composition of the resulting water is shown and, for comparison, the composition of the Arnedillo water. The mass transfers of the considered phases are also shown (positive values mean precipitation whilst negative values mean dissolution).

	Final water (mmol/L)	Arnedillo water (mmol/L)	Mineral phase	Mass transfer (mmol/L)
HCO_3^-	2.84	2.92	**Calcite**	0.5
SO_4	16.2	15.5	**Dolomite**	-0.25
Cl	91.6	91.5	**Anhydrite**	-2.1
Na	88.5	92	**Albite**	0.4
Ca	14.4	11.5	**K-feldspar**	-0.4
Mg	2.9	2.1	**Quartz**	0.01
Si	0.5	0.6		
K	1.2	1.3		

Table 7. Total mass transfers obtained in the reaction-path calculation when 2000 mmol/L of halite are dissolved at pH of 6, 7 and 8 and temperatures of 25, 100 and 200 ºC. The results are expressed in mmol/L (positive values mean precipitation and negative values mean dissolution).

	pH=6			**pH=7**			**pH=8**		
	25ºC	**100ºC**	**200ºC**	**25ºC**	**100ºC**	**200ºC**	**25ºC**	**100ºC**	**200ºC**
Calcite	48.9	5.2	0.5	51.2	5.6	0.6	51.3	5.6	0.8
Dolomite	-23.4	-2.9	-0.4	-26.6	-2.8	-0.4	-26.3	-2.8	-0.4
Anhydrite	-61.3	-21.5	-4.9	-63	-21.7	-4.9	-63	-21.7	-4.9
Albite	1.9	16	77	1.9	16	77	1.9	16	77
K-Feldspar	-1.9	- 16	-77	-1.9	- 16	-77	-1.9	- 16	-77

- Mineral equilibria are evaluated in low temperature geothermal systems
- Geochemical evolution of the waters in the geothermal reservoir is discussed
- Halite dissolution is the triggering factor for the dedolomitisation process
- Halite dissolution produces albitisation